Morphology of Alternating Poly(ester amide)s Based on 1,4-Butylene Established by ^{13}C Solid-State NMR Relaxation Measurements

Peter J. M. Serrano,[†,#] John P. M. van Duynhoven,[‡,§] Reinoud J. Gaymans,*[,†] and Ron Hulst*[,‡,⊥]

Department of Synthesis and Technology of Engineering Plastics, University of Twente, P.O. Box 217, 7500 AE Enschede, The Netherlands; Department of Chemical Analysis, University of Twente, P.O. Box 217, 7500 AE Enschede, The Netherlands; Unilever R&D, Olivier van Noortlaan, 3133 AT Vlaardingen, The Netherlands; and BiOMaDe Technology Foundation, Nijenborgh 4, 9747 AG Groningen, The Netherlands

Received May 6, 2002

ABSTRACT: Alternating poly(ester amide)s consisting of 1,4-butylene and diol spacing entities (4NTm and 4NTm,p) were studied using solid-state NMR techniques. The direct monitoring of the NMR relaxation behavior of different ester and amide moieties suggested a significant impact of spacer length on the molecular dynamics. Crystallization domains of the diol spacers of annealed 4NTm as well as 4NTm,p poly(ester amide)s were identified by means of solid-state CP-MAS ^{13}C $T_{1\rho}$ relaxation measurements. From solid-state ^{1}H $T_{1\rho}$ relaxation measurements, the *thickness* of the lamellae could be estimated including the domain sizes. Quantitative analysis of ^{13}C CP-MAS buildup curves yielded information on the crystallinity of the spacer groups. The macroscopic parameter T_m correlates on a molecular level with (macro)molecular dynamics, thickness of the lamellae, and crystallinity of diol spacers.

Introduction

Alternating poly(ester amide)s of the type 4NT*m* and 4NT*m*,*p* (**1**), consisting of rigid T4T bis(ester diamide)s (dimethyl terephthalate and 1,4-butanediamine) and flexible diol spacer(s) building blocks of differing lengths,[1−3] have not yet been investigated fully in order to assess the morphology[4] (Figure 1).

The 4NT*m* polymers, based on a single diol consisting of *m* methylene groups, crystallized rapidly, exhibiting an odd−even effect with regard to the melting temperatures whereas the odd spaced materials also crystallized to a somewhat smaller extent compared to the even spacer (Figure 2).

The 4NT*m*,*p* polymers, based upon a mixture of diols consisting of *m* and *p* methylene moieties, did not show the odd−even effect in their melting temperature, suggesting that the diols do not (co)crystallize. The 4NT*m* and 4NT*m*,*p* polymers had high glass transition temperatures; only one T_g value was found for the ester and amide units, suggesting that the systems were miscible in the amorphous phase. For the 4NT*m* the T_g follows also an odd−even effect; surprisingly, the odd diols have higher T_g values (Figure 3). For polymers based upon mixtures of diols (4NT*m*,*p*), the T_g decreases steadily with the average diol length, suggesting that the odd−even effect on the amorphous phase is a direct consequence of the odd−even effect of the crystalline phase.

To investigate both the structure and morphology of polymeric materials with the aim of understanding and explaining their dynamic macromolecular properties, several techniques are viable. Among the most widely used are thermal analysis, various forms of (cryo)-electron and atomic force microscopy, and X-ray diffraction. Nuclear magnetic resonance in the solid state is an important technique being highly sensitive to the chemical environment of nuclei and local changes thereof.[5,6] Therefore, NMR is capable of resolving chemical structure and composition and, moreover, of addressing several issues on the dynamic behavior of crystalline as well as amorphous phases/regions within the polymeric materials, including the relative domain dimensions.[7−9]

Aharoni and co-workers[10−12] performed structural studies on liquid crystalline poly(ester amide)s by means

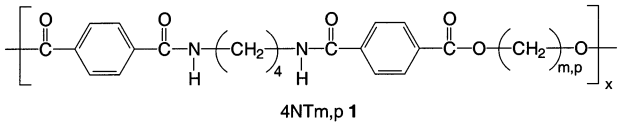

Figure 1. General structure of the polymers used in this study.

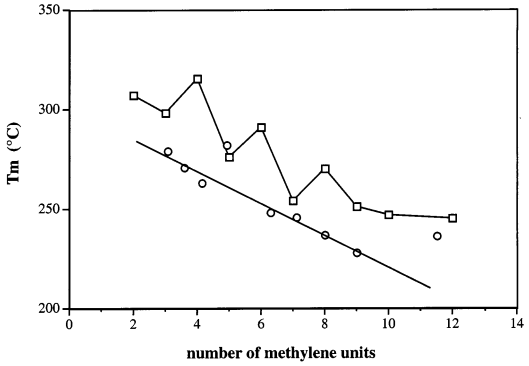

Figure 2. Melting temperature of 4NT*m* (□) and 4NT*m*,*p* (○) polyester amides versus average number of methylene groups in the diol (*m*/*m*,*p*).

* Corresponding authors: e-mail john-van.duynhoven@unilever.com and hulst@biomade.nl.
† Department of Synthesis and Technology of Engineering Plastics, University of Twente.
‡ Department of Chemical Analysis, University of Twente.
§ Unilever R&D.
⊥ BiOMaDe Technology Foundation.
Present address: Loparex BV, Laan van Westenenk 45, P.O. Box 447, 7300 AK Apeldoorn, The Netherlands.

10.1021/ma020689n CCC: $22.00
Published on Web 08/31/2002

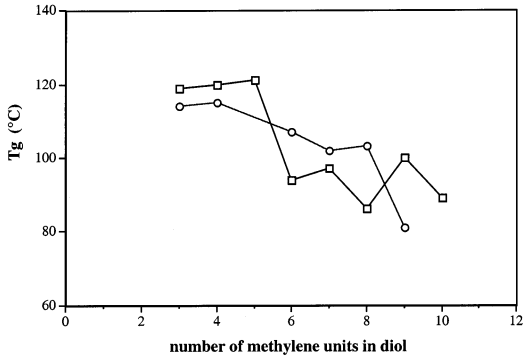

Figure 3. Glass transition temperature (T_g) of 4NT*m* (□) and 4NT*m*,*p* (○) polyester amides vs average number of methylene groups in the diol (*m*/*m*,*p*).

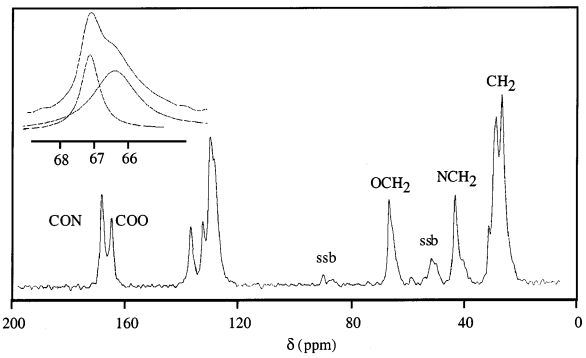

Figure 4. ^{13}C CP-MAS spectrum of 4NT7. *CP*-mix = 2.5 ms, rotor speed 7.9 kHz, ν_1 79 kHz. Spinning sidebands (ssb) are marked. Inset shows expansion of the $-OCH_2-$ moiety resonance, together with the deconvolution pattern. See text for explanation.

of X-ray diffraction as well as MAS solid-state NMR. They were able to assign an overall lamellar structure for the polymers studied. An all-trans conformation for the methylene groups between the amide linkages was found, with the ester methylene groups showing gauche as well as trans conformations, depending on the length of the ester spacer. Gabriëlse and co-workers[13] proposed a three-region model for the poly(ethylene terephthalate) (PET) yarns studied and were able to distinguish between an NMR crystalline, a rigid NMR amorphous, and a mobile NMR amorphous region on the basis of the measurements of the ^{13}C magnetization decay in the rotating frame (^{13}C $T_{1\rho}$). The sizes of the rigid domains, estimated from ^{1}H $T_{1\rho}$ analyses, corresponded well with the crystal sizes determined by X-ray diffraction.

Solid-state NMR was also applied to determine the crystallinity of polymers, e.g. by Veeman and co-workers,[14] who calculated the crystallinity of poly(oxymethylene) via ^{13}C $T_{1\rho}$ measurements monitoring the decay of the ^{13}C magnetization in the rotating frame ($T_{1\rho}$). The $T_{1\rho}$ values found for the crystalline phases were much shorter than the $T_{1\rho}$ values found for the amorphous domains, suggesting that the crystalline $T_{1\rho}$ values were not only determined by pure spin−lattice relaxation mechanisms but also influenced by spin−spin relaxation interactions.

To establish whether the flexible diol spacers of the alternating poly(ester amide)s 4NT*m* and 4NT*m*,*p* do (co)crystallize in defined molecular domains, solid-state MAS NMR relaxation measurements on a series of poly(ester amide)s at various temperatures were performed, paying special attention on the determination of the domain sizes. To overcome the uncertainties with respect to the interpretation of $T_{1\rho}$ data in terms of chain mobility/molecular dynamics, the (relative) contribution of the *spin−spin* and *spin−lattice* relaxation behavior to the "overall" $T_{1\rho}$ times was also established. The results were compared with literature data on comparable compounds and proved to be in promising agreement.

Experimental Section

NMR Spectroscopy. Solid-state NMR measurements were performed on postcondensed powdered (annealed) samples using a Varian Unity 400 WB NMR spectrometer operating at 400 and 100 MHz for ^{1}H and ^{13}C channels, respectively. In all experiments cross-polarization (CP) techniques and high-power proton decoupling were combined with magic angle spinning (MAS) in order to obtain high-resolution ^{13}C NMR spectra. A Jakobsen design probe head with 5 mm ZrO_2 spinners was used in combination with a Sørensen heating apparatus and a Varian rotor speed control unit. The magic angle spinning speeds and applied radio-frequency field strengths (ω_1) ranged from 4 to 9 kHz and 35 to 80 kHz, respectively; recycle delays were 5−8 s. At the applied spinning frequencies overlap of isotropic resonances with spinning sidebands was not observed. Hexamethylbenzene and adamantane were used to adjust the Hartman−Hahn cross-polarization (CP) conditions and as external secondary chemical shift reference, respectively.

^{13}C $T_{1\rho}$ relaxation measurements in the rotating frame were recorded by repeated cycling through a range of different ^{13}C spin-lock times, each cycle adding 64 accumulations and eliminating eventual experimental drift errors caused by spinner instability or by small spectrometer performance fluctuations during the experiment.

^{1}H and ^{13}C $T_{1\rho}$ relaxation measurements were measured by means of Varian pulse programs. Deconvolution of the frequency domain spectra in Lorentzian line shapes was performed using the standard Varian Vnmr software package. ^{13}C $T_{1\rho}$ decay curves are obtained from the monitoring of the ^{13}C resonance intensities as a function of τ.

Results and Discussion

The studied alternating poly(ester amide)s 4NT*m* and 4NT*m*,*p* have T_g values which are all well above room temperature (see Figure 3); the amorphous phases at room temperature are thus in the glassy state.

A. Assignment and Characteristics of the ^{13}C CP-MAS NMR Spectra. Since all the compounds give rise to (some) line broadening and partial overlap of several resonances, the assignments for the 4NT*m* compounds are partly based on comparison with available solution NMR data using closely related, though soluble, materials.[15] Figure 4 shows a typical ^{13}C CP-MAS spectrum for 4NT*m* poly(ester amide)s with $m = 7$ (4NT7).

Unexpectedly, the ^{13}C NMR chemical shifts of the amide units do not vary much for the different 4NT*m* compounds (Figure 5, only the T4T $-NCH_2-$ and $-CO-$ shifts are shown), whereas the $-OCH_2-$ resonances for the diol moiety are shifted significantly downfield upon increasing *m* from 2 to 4. Further increase of *m* does not impose a further downfield shift of the $-OCH_2-$ resonances. In contrast to the amide carbonyl located in the T4T region, the ester carbonyl resonance shows a clear and outspoken odd−even chemical shift effect within the range from 3 to 10 methylene units; the odd−even trend does not include the compound with the ethylene unit ($m = 2$), probably due to the limited ability of this very short chain to adjust to morphological demands.

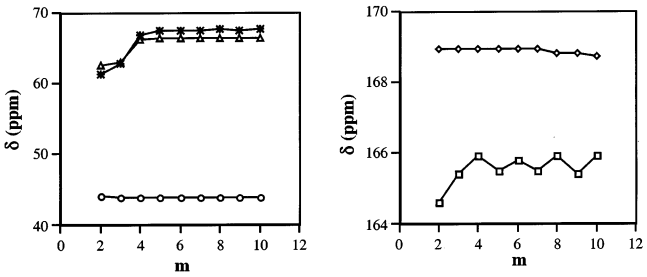

Figure 5. Chemical shifts of the different components in 4NT*m*: crystalline NCH_2 (○) and OCH_2 (*); amorphous OCH_2 (△), COO (□), and CON (◇) resonances.

Clearly, this chemical shift behavior of the ester carbonyl suggests that compounds with odd and even diol lengths are conformationally different.

More detailed study indicated that the $-OCH_2-$ resonances in fact consist of a narrow and broad component, which exact positions were determined via deconvolution in Lorentzian line shapes. Although the ester carbonyl resonances also displayed a narrow and broadening component, the exact positions could not be assessed due to overlap with the amide carbonyl resonance of the T4T moiety.

Upon the use of diols with *m* larger than 4, the broad component is shifted more upfield than the narrow component. In previous studies of poly(butylene terephthalate) (PBT), narrow and broad components corresponded with crystalline and amorphous phases, respectively. The chemical shift difference can be attributed to a γ-gauche anisotropy effect originating from gauche $-OCH_2C-CCH_2-$ bonds in the amorphous diol;[11,16] the downfield shift of the narrow resonance indicates the presence of a trans $-OCH_2C-CCH_2-$ bond. For polymers with $m = 2$, however, the spectral positions of the narrow and broad components are reversed although assignment to respectively crystalline and amorphous components stays viable.[12,13] Aharoni and co-workers[12] suggested that in the crystalline and amorphous regions the $-OCH_2C-CCH_2-$ bonds might also adopt trans and gauche conformations although the aberrant behavior of the ester carbonyl suggests that this polymer presents a special case and does not fit in the conformational behavior observed for diols with *m* larger than 3.

The CP-MAS spectra of the 4NT*m*,*p* polymers reveal also narrow and broad $-OCH_2-$ resonances. The intensities of the amorphous components of the 4NT*m*,*p* polymers are much larger compared to those of 4NT*m* polymers, indicating that the diol moieties have less tendency to cocrystallize with the T4T segments.

Previously, the $-OCH_2-$ resonance has been utilized as a "monitor" for the structure and dynamics of diol spacers (PBT,[17,18] PET,[13,19] and poly(ester amides)[11,12]), and this prompted us to elaborate a cocrystallization model in terms of mobility of the diol moiety, the dimensions of the crystalline domains, and the crystallinity of the diol spacers.

B. Relaxation Measurements. *Introduction*. NMR relaxation times provide information concerning dynamic behavior ranging from the hertz to megahertz frequency range. This affords valuable information on the mobility and molecular packing of molecular distinct regions in the crystalline and amorphous phases within the polymers. In the current study we monitored the spin−lattice relaxation times in the rotating frame, $T_{1\rho}$, that relates to molecular dynamics according to

$$\frac{1}{T_{1\rho}^{SL}} = \frac{1}{20}\gamma_H^2\gamma_C^2\frac{h}{2\pi}\sum r_i^{-6}\left(\frac{4\tau_C}{1+\omega_1^2\tau_C^2}+\frac{\tau_C}{1+(\omega_H-\omega_C)^2\tau_C^2}+\frac{3\tau_C}{1+\omega_C^2\tau_C^2}+\frac{6\tau_C}{1+(\omega_H+\omega_C)^2\tau_C^2}+\frac{6\tau_C}{1+\omega_H^2\tau_C^2}\right) \quad (1)$$

in which τ_C is the random isotropic rotation correlation time for the $^{13}C-^1H$ pair vector, ω_H and ω_C are the Larmor frequencies for the ^1H and ^{13}C nuclei, and γ_H and γ_C are the corresponding gyromagnetic constants. In this theoretical description we assume isotropic tumbling for the vector connecting the nuclei (length given by r_j). Isotropic tumbling is unlikely to occur in solids, but here we merely use τ_C as a measure for the dynamics of the connecting vector (r_j). The variable ω_1 accounts for the strength of the applied spin-lock field often given as $\nu_1 = \omega_1/2\pi$. The measured relaxation times in the rotating frame comprise of spin−lattice and spin−spin relaxation contributions, of which the latter is largely enhanced in rigid semicrystalline materials.[14,19] Because of this, the overall $T_{1\rho}$ consists of two components according to

$$\frac{1}{T_{1\rho}} = \frac{1}{T_{1\rho}^{SL}} + \frac{1}{T_{1\rho}^{SS}} \quad (2)$$

Typically, the ^{13}C spins measured in ^{13}C $T_{1\rho}$ experiments are coupled to the lattice in two distinguishable ways; in both mechanisms the ^{13}C spins are coupled to the proton-induced fluctuating local magnetic fields. Molecular motions modulating with the $^{13}C-^1H$ dipolar coupling give rise to fluctuating fields described by the normal spin−lattice relaxation time constant $T_{1\rho}^{SL}$ for the ^{13}C nuclei. The strong $^1H-^1H$ dipolar interactions, giving rise to fast proton−proton spin flip-flops, are described by the spin−spin relaxation time constant $T_{1\rho}^{SS}$, which becomes more important for rigid crystalline segments and/or systems with short internuclear $^1H-^1H$ and $^{13}C-^1H$ distances. For measurements under the magic angle, the spin−spin contribution can be described by T_{CH}^{D}, the time constant of the coupling between the ^{13}C nuclei and the dipolar reservoir.[20,21] T_{CH}^{D} is in exponential relation with the ω_1 field according to

$$T_{1\rho}^{SS} \approx T_{CH}^{D} \sim \epsilon^{\varpi_1\tau_D} \quad (3)$$

so

$$\frac{1}{T_{1\rho}} \approx \frac{1}{T_{1\rho}^{SL}} + \frac{1}{T_{CH}^{D}} \quad (4)$$

in which τ_D is the dipolar fluctuation time. Measurements performed at incremented spin-lock field strengths ω_1 (ν_1) allow the determination of the different contributions of the relaxation to $T_{1\rho}^{SS}$ and hence $T_{1\rho}$ times.

^{13}C $T_{1\rho}$ Relaxation Measurements. The decay curves of the ^{13}C magnetization of the crystalline and amorphous component of the $-OCH_2-$ resonance of poly(ester amide) 4NT8 in the rotating frame show different relaxation rates. The amorphous component relaxes faster compared to the crystalline component, in agreement with the expectation that chains in the amorphous

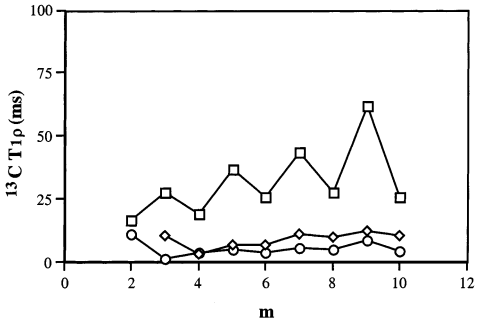

Figure 6. ^{13}C $T_{1\rho}$ decay of the narrow (□) and broad (◇) components of the -OCH_2− line shapes as a function of the diol spacer lengths *m* for the 4NT*m* polymers. Recorded with $\nu_1 = 79$ kHz, rotor speed = 7.9 kHz. Also shown the values for the narrow component at $\nu_1 = 55$ kHz and a rotor speed = 6.0 kHz (○).

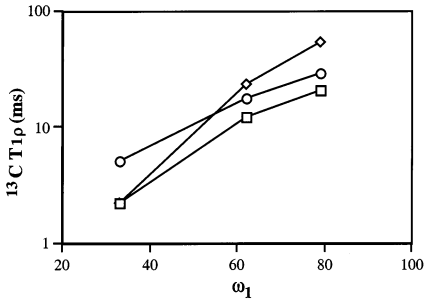

Figure 7. Field strength (ν_1) dependence of ^{13}C $T_{1\rho}$ (at RT) for the crystalline components of 4NT9 (◇) and 4NT10 (□). Also shown the expected (calculated) dependency for spin−lattice contribution only to $T_{1\rho}$ (○).

phase are more mobile, and the magnetizations of the nuclei involved thus relax more readily.

The $T_{1\rho}$ relaxation data of the broad and narrow components of the −OCH_2− resonances of 4NT*m* polymers are summarized as a function of the diol spacer length *m* in Figure 6.

At increased spin-lock field strength (ν_1) the relaxation times of the narrow −OCH_2− resonance component are all of the same magnitude. Increase of ν_1 results in increased $T_{1\rho}$ relaxation times, which effect is more pronounced for polymers with odd diol spacer lengths (*m* is odd).

When only spin−lattice relaxation contributes to $T_{1\rho}$, the odd−even effect described suggests a *higher* mobility of the diol spacers in the crystalline phase for the even spaced polymers (*m* is even), which contrasts with the melting temperatures found (T_m).[2] Polymers with even diol spacers clearly had higher T_m values than the polymers with odd spacers. These findings were attributed to thicker lamellae and, hence, a denser packing of the crystalline phase for the even spaced polymers (compared to the odd spaced), implying the even spaced diol spacers to be *less* mobile in the crystalline phase. To verify whether the behavior suggested by the ^{13}C $T_{1\rho}$ measurements is caused by a (larger) contribution of spin−spin diffusion to the $T_{1\rho}$ values for the even spaced poly(ester amide)s, measurements were conducted at different spin-lock field strength's ν_1 for 4NT9 and 4NT10. The increase of $T_{1\rho}$ with increasing field strength's is larger than expected on the basis of spin−lattice contribution solely ($\sim\nu_1^2$), as visualized in Figure 7. Thus, there is a contribution of the spin−spin relaxation to the observed $T_{1\rho}$ values ($\sim \exp(\nu_1\tau_D)$).

The initial slope of the applied spin-lock field strength dependencies of 4NT9 is larger than the initial slope of

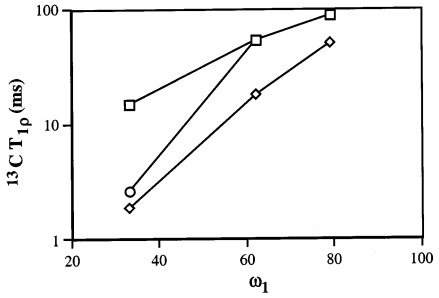

Figure 8. Expected (calculated) field strength (ν_1) dependencies for (a) exclusive spin−lattice contribution to $T_{1\rho}$ (□) and mixed contributions of spin−lattice and (b) strong ($\tau_D = 20$ μs) (◇) and (c) weak ($\tau_D = 60$ μs) (○) spin−spin relaxation.

4NT10 (Figure 7) and is influenced by a larger τ_D value for the 4NT9 polymer. This was verified by model calculations (Figure 8) in which the spin-lock field strength dependencies for spin−lattice and strong ($\tau_D = 20$ μs) as well as weak(er) spin−spin ($\tau_D = 60$ μs) contributions on the overall $T_{1\rho}$ value were determined.

It is concluded that the ^{1}H−^{1}H dipolar interactions in the crystalline domains are weaker in the polymer 4NT9 than in polymer 4NT10, again suggesting a less dense packing of the crystalline phase of the odd spaced polymers compared to the packing of the crystalline phase of the even spaced compounds. The odd−even chemical shift behavior of the carbonyl resonance (vide supra) also suggests that the diols indeed adopt different conformations in the odd and even spaced polymers, which is in agreement with the explanation given for the odd−even effects found for the melting temperatures of the 4NT*m* poly(ester amide)s.[2,22]

^{13}C $T_{1\rho}$ Relaxation Measurements near T_g. The interpretation of the ^{13}C $T_{1\rho}$ data is further sustained by measurements near T_g. Spin−spin relaxation is quenched considerably under these conditions enhancing spin−lattice relaxation processes. Accordingly, for the *crystalline* components, short(er) relaxation times are observed for polymers with odd diol spacer lengths, although the effects are most outspoken for spacer length values exceeding $m = 7$ (vide infra). Therefore, spin−lattice processes largely determine the magnetization decay at 100 °C, and the observed relaxation times are pure spin−lattice parameters.

Evidently, the odd−even effect is reversed near T_g and similar to the effect found for T_m whereas the mobility of the −OCH_2− moiety in the crystalline phase is less for even spaced poly(ester amide)s compared to the odd spaced polymers. The macroscopic parameter T_m thus appears to be reflected on a molecular level in terms of the mobility of polymer segments in the crystalline phase, visualized by the τ_c as determined through ^{13}C $T_{1\rho}$.

The odd−even effect of the $T_{1\rho}$ values (vide supra) becomes more pronounced for elongated spacer lengths as the interchain interactions (hydrogen bonds) decrease with increasing diol spacer length. The factors governing the odd−even effect thus become more prevalent and changes in the molecular dynamics more pronounced.[11]

For the 4NT*m*,*p* poly(ester amide)s, similar relaxation experiments were performed at ambient temperature (Figure 10). In Figure 10, the average diol spacer length is given, and the relaxation times of a polymer with an even *m* value thus average the values of two odd diol spacers. Polymers with a diol mixture of odd spacer lengths show again a higher $T_{1\rho}$ value, which can be

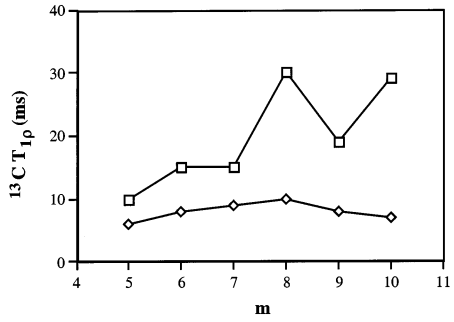

Figure 9. ^{13}C $T_{1\rho}$ decay of narrow (□) and broad (◇) component of the $-OCH_2-$ line shapes observed for the different 4NT*m* polymers as a function of the diol length (*m*) at 100 °C. All relaxation measurements were performed at ν_1 = 79 kHz and rotor speed = 7.9 kHz.

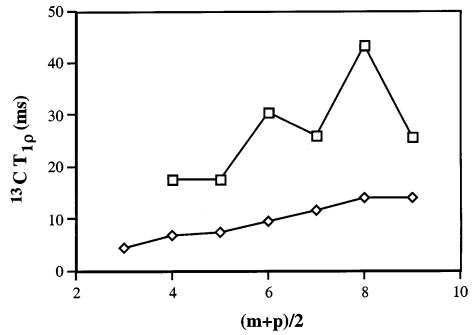

Figure 10. ^{13}C $T_{1\rho}$ times of polymers 4NT*m*,*p* for the narrow (□) and broad (◇) component of the $-OCH_2-$ line shapes as a function of the average diol length ((*m* + *p*)/2) at room temperature. Recorded with ν_1 = 79 kHz and rotor speed of 7.9 kHz.

explained in terms of smaller spin−spin contributions. Moreover, it is clear that within the 4NT*m*,*p* poly(ester amide) series, which contain mixtures of diols, the diol moieties also crystallize to some extent.

The relaxation behavior of the *amorphous* components of the 4NT*m* and the 4NT*m*,*p* polymers show a less pronounced behavior as a function of the (average) diol spacer length compared to the crystalline components. Generally, the $T_{1\rho}$ values of the amorphous components are shorter compared to the crystalline parts, and consequently the diols in the amorphous phase reveal more dynamic behavior.[13]

Addressing Domain Sizes Using ^1H $T_{1\rho}$ Relaxation Measurements. The ^1H relaxation times in the rotating frame were measured in an indirect manner by monitoring the intensity of the ^{13}C resonances (see Experimental Section). The decay curves of the different ^{13}C NMR resonances appear to be very similar, which can be explained by the averaging effect of spin diffusion on the intrinsic ^1H $T_{1\rho}$ relaxation times of the respective protons. In the $T_{1\rho}$ decay curves, a faster as well as a more slowly relaxing component can be discerned, suggesting the presence of a heterogeneous polymer structure.

It is suggested that the total ^1H magnetization decay follows a pathway schematically represented in Figure 11. In this model, a one-dimensional two-region system consisting of one crystalline (C) and one amorphous (A) phase only is assumed. The amorphous phase is characterized by very short intrinsic $T_{1\rho}$ values, whereas the $T_{1\rho}$ values of the crystalline phases are much longer. This implies that the magnetization of the mobile amorphous phase decays fast whereas the magnetization in the rigid domains will decay more slowly, as indicated in Figure 11 by the broad and narrow arrows.

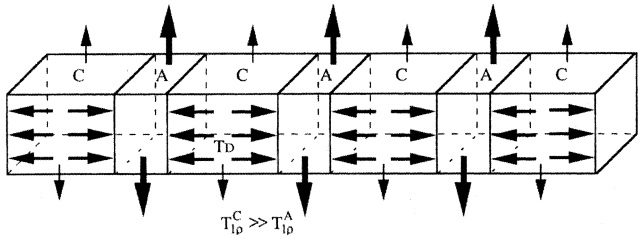

Figure 11. Schematic representation of ^1H $T_{1\rho}$ in a heterogeneous (crystalline (C) and amorphous (A)) system with two distinct intrinsic decay rates ($T_{1\rho}^C$ and $T_{1\rho}^A$) and a magnetization diffusion rate in the rigid phase T_D. Broader arrows indicate higher magnetization fluxes.

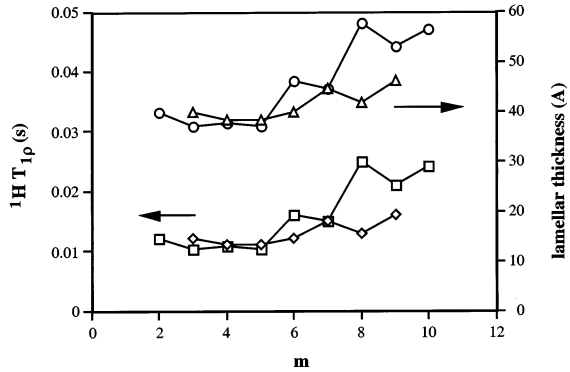

Figure 12. (a) ^1H $T_{1\rho}$ values for the slow components of 4NT*m* (□) and 4NT*m*,*p* (◇) polymers vs average diol length (*m*). (b) Calculated data for the lamellar thickness as discussed in the text (4NT*m* (○), 4NT*m*,*p* (△)).

However, if the magnetization decay is less effective and $T_{1\rho}$ much longer than the diffusion time of the magnetization to the mobile phase, diffusion of the magnetization of the rigid to the mobile phase, which acts as a "relaxation sink", will occur: the effective $T_{1\rho}$ component measured for the crystalline phase is now determined by diffusion.[23,24] From this $T_{1\rho}$, determined by diffusion of the magnetization from the crystalline to the amorphous phase and not by intrinsic relaxation processes in the crystalline phase, the domain sizes can be calculated.[25,26] The dimensionality of the domains is a necessary parameter in order to access the domain sizes. It is known, however, that these kind of poly(ester amide)s usually crystallize in lamellae.[27−29] Assuming a lamellar orientation of the consecutive domains, the following formula can be used to determine the domain size for a one-dimensional two-region system:[30]

$$l = 2\{1.33 D_{1\rho} T_{1\rho}\}^{1/2} \qquad (5)$$

in which l is the lamellar thickness, $D_{1\rho}$ the diffusion constant (in the rotating frame), and $T_{1\rho}$ the effective measured $T_{1\rho}$ of the crystalline component during the experiment. The diffusion constant $D_{1\rho}$ depends on the chemical structure of both phases and is for the system currently studied unknown. By assuming uniform domain sizes and diffusion constants, however, we were able to calculate the lamellar thickness for the 4NT*m* and 4NT*m*,*p* polymers using the literature D_1 value for PET (5×10^{-16} m^2 s^{-1}).[30] In a ^1H $T_{1\rho}$ experiment where spin diffusion evolves under the influence of an on-resonance radio-frequency field on the proton channel, the spin-diffusion coefficient is half the value of that in

laboratory frame.[30,31] Therefore, a reasonable estimation for $D_{1\rho}$ is 2.5×10^{-16} m^2 s^{-1}.

Aharoni and co-workers[10−12] also studied poly(ester amide)s with X-ray diffraction methods. They found an increase of the lamellar thickness of only 0.2−0.3 Å on average per methylene unit for the first five spacing methylene groups in the ester part, which was explained by the incorporation of methylene groups in the gauche conformation. The following methylene groups were incremented 1.2−1.4 Å per entity, which is indicative for an average trans conformation. When using these data in the next equation,

$$l = 19.5 + 2.52\{0.5(m + 1)\} \quad (6)$$

in which l is the lamellar thickness and m the (average) number of methylene groups in the diol spacer entity, the values for the thickness of the lamellae change slightly. The best fit for the 4NT*m* polymers is in between one or two spacer groups and two T4T segments. The 4NT*m*,*p* polymers show the best fit with two T4T segments and one spacer group. The differences in the thickness of the lamellae are only small, especially for polymers with relatively short diol spacer lengths. Clearly, these results have to be treated carefully especially facing the underlying assumptions (uniform domain size and diffusion $D_{1\rho}$, lamellar geometry).

It is tempting to conclude that the thickness of the lamellae of the 4NT*m* poly(ester amide)s is somewhat larger compared to the 4NT*m*,*p* poly(ester amide)s although the lamellar thickness for polymers with short spacer groups is almost equal for both systems. These findings may be caused by the gauche conformations of the diol spacers, leading to only small increments per added methylene moiety. Also, with shorter spaced diol moieties, a critical lamellar thickness may be reached for which the model-based assumptions are no longer valid. With larger spacer groups, the thickness of the lamellae of the 4NT*m* polymers increases due to the crystallization of a second spacer moiety. For the 4NT*m*,*p* polymers this crystallization is probably hindered considerably by the different lengths of the spacing entities. The differences in the lamellar thickness of the odd and even spaced polymers 4NT*m* are, however, too small to be explained in terms of differences in the melting points solely. The packing of the chains has, likely, a distinctive influence on T_m as the even spaced polymers have the more dense packing.

^{13}C CP-MAS Buildup Measurements. With the aid of ^{13}C CP-MAS buildup curves an attempt is made to quantify the molar ratios of the *crystalline* and *amorphous* components and thus the crystallinity of the polymer.[32] In Figure 13, several of the buildup curves for the $-OCH_2-$ resonance are collected.

Unfortunately, only for poly(ester amide)s with long(er) spacer lengths were reliable values obtained. The crystallinity of the diol spacing moieties of the 4NT*m* polymers shows again an odd−even effect, the even spaced polymers having the higher crystallinity in agreement with the T_m measurements (vide supra). As expected, the diol spacing entities in the 4NT*m*,*p* poly(ester amide)s crystallize to a much lesser extent. An injection of a molded sample of poly(ester amide) 4NT5,7 did not show any crystallization of the diol spacer. The crystallinity of the diol spacing entities as obtained by NMR measurements are much higher than the values found with DSC.[2] We note that with DSC analysis the second heating scan is used to determine the ΔH_m values, whereas the NMR measurements were performed on postcondensated "annealed samples".

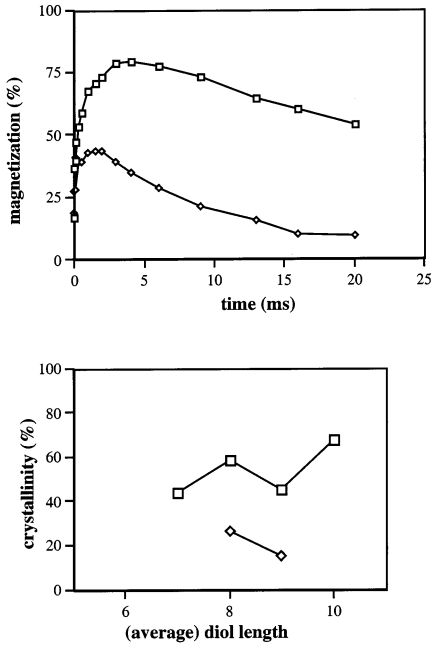

Figure 13. Cross-polarization buildup curves observed for 4NT9 at $\nu_1 = 79$ kHz and rotor speed of 7.9 kHz crystalline (□) and amorphous (◇) components (upper). Fraction of crystalline magnetization present as determined from quantitative analysis of CP buildup rates for poly(ester amide)s 4NT*m* (□) and 4NT*m*,*p* (◇) (lower).

Conclusions

Crystallization domains of the diol spacers of annealed 4NT*m* as well as 4NT*m*,*p* poly(ester amide)s were identified by means of solid-state CP-MAS ^{13}C $T_{1\rho}$ relaxation measurements. An odd−even effect in the crystalline diol spacing components of the polymers was observed, and it was concluded that packing of the even spaced polymers was of a higher density than that of the odd spaced polymers. These results indicate a more efficient crystallization of the diol spacers for even spaced polymers compared to the odd spaced polymers.

From solid-state ^{1}H $T_{1\rho}$ relaxation measurements, the thickness of the lamellae could be estimated. The ^{1}H $T_{1\rho}$ decay consisted of a fast relaxing component (amorphous phase) and a slow relaxing component (crystalline phase). Assuming a one-dimensional two-region (model) system, uniform lamellae and uniform diffusion constant, the lamellae were found to consist of two T4T segments and one spacer group for the 4NT*m*,*p* polymers and of two T4T segments and two spacer groups for the 4NT*m* polymers on average. The 4NT*m* polymers appeared to be built up of slightly thicker lamellae compared to the 4NT*m*,*p* polymers. With an identical overall crystallinity (based on DSC) this indicated that the 4NT*m*,*p* polymers crystallize with more lamellae than the 4NT*m* polymers. Values for the thickness of the lamellae ranged from 37 to 56 Å, typically.

Quantitative analysis of ^{13}C CP-MAS buildup curves yielded information on the crystallinity of the spacer groups. The spacing diols of the 4NT*m* polymers had a higher crystallinity compared to the spacer moieties of the 4NT*m*,*p* polymers. Again, an odd−even effect was found for the crystallinity of the 4NT*m* poly(ester amide)s, in agreement with other NMR experiments.

This confirmed the melting temperature behavior reported earlier.

In conclusion, solid-state CP-MAS NMR analysis can be applied to describe the macroscopic parameter T_m on a molecular level through the correlation times τ_C, thickness of the lamellae, and crystallinity of diol spacers.

References and Notes

(1) Serrano, P. J. M.; van Bennekom, A. C. M.; Gaymans, R. J. *Polymer* **1998**, *39*, 5773. Serrano, P. J. M.; Thüss, E.; Gaymans, R. J. *Polymer* **1997**, *38*, 3893. Serrano, P. J. M.; van de Werff, B. A.; Gaymans, R. J. *Polymer* **1998**, *39*, 83.

(2) Serrano, P. J. M.; Gaymans, R. J.; Aerts, L. *Polymer* **1998**, *39*, 2291.

(3) The alternating poly(ester amide)s (4NT*m* and 4NT*m*,*p*) are based on polyamide 4,T units (4N) and a polyterephthalate units (T*m* or T*m*,*p*); *m* and *p* stand are the number of methylene units in the diol moiety. With 4NT*m*,*p* a mixture of diols was used with length *m* and *p*, respectively.

(4) For a comparable study on the poly(ester amide)s with diverging building blocks see: Stapert, H. R.; Dijkstra, A.; Dijkstra, P. J.; Feijen, J.; van Duynhoven, J. P. M.; Hulst, R. *Macromolecules*, submitted.

(5) Koenig, J. L. In *Spectroscopy of Polymers*; American Chemical Society: Washington, DC, 1992.

(6) Schafer, J.; Stejskal, E. O.; Buchdahl, R. *Macromolecules* **1977**, *10*, 384.

(7) Spiess, H. W. *Annu. Rev. Mater. Sci.* **1991**, *21*, 131.

(8) Spiess, H. W. *Chem. Rev.* **1991**, *91*, 1321.

(9) Part 2: Hulst, R.; Seyger, R.; van Duynhoven, J. P. M.; van der Does, L.; Noordermeer, J. W. M.; Bantjes, A. *Macromolecules* **1999**, *32*, 7509. Part 3: Hulst, R.; Seyger, R.; van Duynhoven, J. P. M.; van der Does, L.; Noordermeer, J. W. M.; Bantjes, A. *Macromolecules* **1999**, *32*, 7521.

(10) Murthy, N. S.; Aharoni, S. M. *Macromolecules* **1992**, *25*, 1177.

(11) Hatfield, G. R.; Aharoni, S. M. *Macromolecules* **1989**, *22*, 3807.

(12) Aharoni, S. M.; Correale, S. T.; Hammond, W. B.; Hatfield, F. R.; Murthy, N. S. *Macromolecules* **1989**, *22*, 1137.

(13) Gabriëlse, W.; Gaur, H. A.; Feyen, F. C.; Veeman, W. S. *Macromolecules* **1994**, *27*, 5811.

(14) Veeman, W. S.; Menger, E. M.; Ritchey, W.; de Boer, E. *Macromolecules* **1979**, *12*, 924.

(15) Serrano, P. J. M.; Gaijmans, R. J., unpublished results.

(16) Silvestri, R. L.; Koenig, J. L. *Anal. Chim. Acta* **1993**, *283*, 997.

(17) Jelinski, L. W.; Dumais, J. J.; Engel, A. K. *Macromolecules* **1983**, *16*, 403. Jelinski, L. W.; Dumais, J. J.; Watnick, P. I.; Engel, A. K.; Sefcik, M. D. *Macromolecules* **1983**, *16*, 409.

(18) Gomez, M. A.; Cozine, M. H.; Tonelli, A. E. *Macromolecules* **1988**, *21*, 388.

(19) Sefcik, M. D.; Schaefer, J.; Stejskal, E. O.; McKay, R. A. *Macromolecules* **1980**, *13*, 1132.

(20) VanderHart, D. L.; Garroway, A. N. *J. Chem. Phys.* **1979**, *71*, 2773.

(21) Garroway, A. N. *J. Magn. Reson.* **1979**, *34*, 283.

(22) Kinoshita, Y. *Macromol. Chem.* **1959**, *33*, 1.

(23) Packer, K. J.; Pope, J. M.; Yeung, R. R. *J. Polym. Sci., Polym. Phys. Ed.* **1984**, *22*, 589.

(24) Kenwright, A. M.; Packer, K. J.; Say, B. J. *J. Magn. Reson.* **1986**, *69*, 426.

(25) Booth, A. D.; Packer, K. J. *Mol. Phys.* **1987**, *62*, 811.

(26) Demco, D. E.; Johansson, A.; Tegenfeldt, J. *Solid-State Nucl. Magn. Reson.* **1995**, *4*, 13.

(27) Perego, G.; Cesari, M.; Della Fortuna, G. *J. Appl. Polym. Sci.* **1984**, *29*, 1141.

(28) Van Hutten, P.; Mangnus, R. M.; Gaymans, R. J. *Polymer* **1993**, *34*, 4193.

(29) Van Bennekom, A. C. M. Fast Crystallizing Polyesteramides. Ph.D. Thesis, University of Twente, 1995.

(30) Havens, J. R.; VanderHart, L. D. *Macromolecules* **1985**, *18*, 1663.

(31) Henrichs, P. M.; Tribone, J.; Massa, D. J.; Hewitt, J. M. *Macromolecules* **1988**, *21*, 1282.

(32) Stejskal, E. O.; Schaefer, J.; Sefcik, M. D.; McKay, R. A. *Macromolecules* **1981**, *14*, 275.

MA020689N